HHS Public Access

Author manuscript

Neuroimage. Author manuscript; available in PMC 2015 December 02.

Published in final edited form as:

Neuroimage. 2010 August 1; 52(1): 186–197. doi:10.1016/j.neuroimage.2010.04.033.

Joint analysis of structural and perfusion MRI for cognitive assessment and classification of Alzheimer's disease and normal aging

Duygu Tosun[a,*], **Pouria Mojabi**[a], **Michael W. Weiner**[a,b], and **Norbert Schuff**[a,b]

[a]Center for Imaging of Neurodegenerative Diseases, Department of Veterans Affairs Medical Center, San Francisco, CA, USA

[b]Department of Radiology, University of California, San Francisco, CA, USA

Abstract

Structural magnetic resonance imaging (MRI) of brain tissue loss and physiological imaging of regional cerebral blood flow (rCBF) can provide complimentary information for the characterization of brain disorders, such as Alzheimer's disease (AD) but studies into gains in classification power for AD using these image modalities jointly have been limited. Our aim in this study was to determine the joint contribution of structural and perfusion-weighted imaging for the classification of AD in a cross-sectional study using an integrated multimodality MRI processing framework and a cortical surface-based analysis approach. We used logistic regression analysis to determine sequentially the value of cortical thickness, rCBF, and cortical thickness and rCBF jointly for classification for diagnosis of AD compared to controls. We further tested the extent to which cortical thinning and reduced rCBF explain individually or together variability in dementia severity. Separate analysis of structural MRI and perfusion-weighted MRI data yielded the well-established pattern of cortical thinning and rCBF reduction in AD, affecting predominantly temporo-parietal brain regions. Using structural MRI and perfusion-weighted MRI jointly indicated that cortical thinning dominated the classification of AD and controls without significant contributions from rCBF. However there was also a positive interaction between reduced rCBF and cortical thinning in the right superior temporal sulcus, implying that structural and physiological brain alterations in AD can be complementary. Compared to reduced rCBF, regional cortical thinning better explained the variability in dementia severity. In conclusion, structural brain alterations compared to physiological variations are the dominant features of MRI in AD.

Introduction

Most neurodegenerative disorders, such as Alzheimer's disease (AD) and other types of dementia, are associated with characteristic patterns of regional brain alterations that can be visualized using neuroimaging. Moreover, the patterns of structural, functional, and physiological alterations can be regionally discordant, suggesting that each pattern may

*Corresponding author. Center for Imaging Neurodegenerative Diseases, Department of Veterans Affairs Medical Center, 4150 Clement St, Blg 13, 114M, San Francisco, CA 94121, USA. Fax: +1 415 668 2864., duygu.tosun@ucsf.edu (D. Tosun).

provide complementary information (Hayasaka et al., 2006). In AD, for example, structural MRI studies consistently revealed a pattern of brain tissue loss that predominantly involves structures in the medial temporal cortex (i.e., hippocampus and the entorhinal cortex (deToledo-Morrell et al., 2004; Morra et al., 2008, 2009a,b; Schroeter et al., 2009; Stoub et al., 2005; Thompson et al., 2004)), consistent with the known distribution of early AD pathology from histopathological studies (Braak and Braak, 1991). As the severity of AD progresses, structural MRI also shows a gradual expansion of tissue loss into temporo-parietal cortical areas (Chetelat and Baron, 2003; Desikan et al., 2008; Hua et al., 2008a; Whitwell et al., 2007, 2008). On the other hand, functional studies in AD using positron emission tomography (PET) for measurements of cerebral glucose consumption or single photon emission computed tomography (SPECT) and more recently arterial spin labeling magnetic resonance imaging (ASL-MRI) for measurements of regional cerebral blood flow (rCBF) generally found the most prominent alterations in the association cortices (Alsop et al., 2008; Callen et al., 2002; Nebu et al., 2001; Rodriguez et al., 2000), spatially separated from the main structural changes. The affected areas include the posterior temporal and parietal association cortices (Bradley et al., 2002; Keilp et al., 1996; Schroeter et al., 2009), as well as in the posterior cingulate, precuneus, and medial temporal cortices (Asllani et al., 2008; Du et al., 2006; Ishii et al., 1996; Johnson et al., 2005; Kobayashi et al., 2008; Warkentin et al., 2004). However, functional alterations can also be seen in mesial temporal lobe structures and the hippocampus (Alsop et al., 2008; Mosconi et al., 2005), in overlap with early structural changes in these regions. The diversity of these patterns is of clinical interest as it may help separating AD from normal aging as well as staging of the disease, since the patterns generally correlate with the progression of clinical symptoms, especially with decline in memory function (Arbizu et al., 1997; Basso et al., 2006; Benoit et al., 1999; Bruen et al., 2008; Gilboa et al., 2005; Jagust et al., 1989; Keilp et al., 1996; Lampl et al., 2003; Leube et al., 2008; Maestu et al., 2003; Mungas et al., 2005; Nobili et al., 2005, 2007; O'Brien et al., 1992; Reed et al., 1989; Rémy et al., 2005; Rodriguez et al., 1999, 2000; Sabbagh et al., 1997; Schwartz et al., 1991; Wolfe et al., 1995). However, most imaging studies have exploited structural or physiological alterations separately for the classification of AD patients and healthy subjects. Moreover, among studies that used structural and physiological changes together for classification (Jagust, 2006; Kawachi et al., 2006; Matsunari et al., 2007), many ignored potential interactions between structural and physiological changes and often limited the analysis to predetermined regions of interest, potentially under-utilizing information available with imaging.

Our overall goal in this study was to assess in full the value added by using jointly MRI measures of regional cortical thinning and rCBF, including their interaction, for the classification of AD patients and elderly controls. To avoid regional bias, we further aimed to determine the joint classification power of structural and perfusion MRI on a point-by-point basis. In addition to mere group classification, we also aimed to determine the joint value of cortical atrophy and rCBF measures in explaining the variance in the severity of cognitive impairment in AD.

Toward these study goals, we present an integrated multimodality image processing and analysis framework for an effective joint analysis of regional cortical thinning and rCBF variations on a point-by- point basis across the whole brain. Since we are mainly interested

in cortical alterations, pertaining cortical thinning and cortical rCBF, we pursued a cortical surface-based analysis approach, which provides better spatial normalization of cortical data across subjects compared to voxel-based approaches (Tosun and Prince, 2008). In addition, the dense analysis of cortical atrophy and rCBF on cortical surface representations benefits a data-driven approach that overcomes the restrictions of region-of-interest-based methods. Similar cortical surface-based approaches were reported recently for analysis of fMRI data (Anticevic et al., 2008; Hagler et al., 2006; Hashikawa et al., 1995). However, this is – to our knowledge – the first investigation aimed to evaluate structural and perfusion alterations in AD together by using an integrated multimodality MR image-processing framework coupled with 3D cortical surface-based data analysis. In the following sections, the technical challenges for an integrated multimodality MR image-processing framework are described, especially in the context of dementia, where extensive brain atrophy requires accurate spatial alignment of the intra-subject inter-modality MR images, including corrections for nonlinear geometric distortions and partial volume effects in the low-resolution perfusion images. We then present a logistic regression analysis to determine sequentially the value of cortical thickness, rCBF, and cortical thickness and rCBF jointly for the classification of AD patients and cognitively normal controls. We further test the extent to which cortical thinning and reduced rCBF explain individually or together severity of cognitive impairment in AD.

Subjects and methods

Subjects

The study included 38 healthy elderly subjects, aged 51–81 years with Mini-Mental State Examination (MMSE) scores between 26 and 30, and 24 patients diagnosed with Alzheimer's disease, aged 51–85 years with MMSE scores between 8 and 29. All subjects were recruited from the Memory and Aging Center of the University of California, San Francisco and had extensive physical, neurological, and neurocognitive examinations at the center. The MR images were used to rule out other major neuropathologies such as tumors, strokes, or inflammation but not to diagnose dementia. AD patients were diagnosed according to the criteria of the National Institute of Neurological and Communicative Disorders and Stroke-Alzheimer's Disease and Related Disorders Association (NINCDS/ADRDA). All subjects or their legal guardians gave written informed consent before participating in the study, which was approved by the Committees of Human Research at the University of California at San Francisco and the VA Medical Center. Detailed demographics statistics of each group are given in Table 1.

Data acquisition

All scans were performed on a 4 Tesla (Bruker/Siemens) MRI system with a birdcage transmit and 8 channel receive coil arranged in the same housing. The scans included T1-weighted (T1w) and T2-weighted (T2w) structural MRI data for measurements of brain atrophy and perfusion-weighted MRI for measurements of rCBF. T1w images were obtained with a 3D volumetric magnetization prepared rapid gradient echo (MPRAGE) sequence, TR/TE/TI=2300/3/950 ms, timing; 7° flip angle; $1.0\times1.0\times1.0$ mm^3 resolution; 157 continuous sagittal slices; acquisition time of 5 min. T2w images were acquired with a

variable flip (VFL) angle turbo spin-echo sequence with TR/TE=4000/30ms and with the same resolution matrix and field of view of MPRAGE.

Perfusion-weighted MR images were acquired using continuous arterial spin labeling (cASL-MRI) sequence with single-shot echoplanar imaging (EPI), yielding sixteen 5 mm thick slices with 1.2 mm gaps and with an in-plane resolution of $3.75\times3.75\ mm^2$. EPI timing was TR/TE=5200/9 ms (Detre et al., 1992). For cASL, a 1.2 s long pulse with a magnetic field strength of $B_1=3.5\times10^{-6}$ T was applied in the presence of a constant magnetic field gradient of 2 mT/m, followed by 1590 ms post-labeling delay before the signal was mapped using EPI. Post-labeling delay of 1590 ms was heuristically chosen to compensate for the prolonged arterial transit times in this age group (Detre and Alsop, 1999; Hunter et al., 1989). Note, since the acquisition of ALS is slice selective, the post-labeling delay increases linearly for each slice by about 45 ms. The labeling slice was fixed at 80 mm distance inferior to the central imaging slice and anatomically located slightly below the circle of Willis. Forty control and 40 label scans were averaged to boost the signal-to-noise ratio resulting in a total scan time for cASL of about 7 min.

Cognitive assessment

The MMSE was administered to each subject to obtain a summary measure of global cognitive status (Folstein et al., 1975). To achieve a linear discrimination across the entire cognitive range, the MMSE (30 items) scores were nonlinearly transformed to an ability range, as described in Mungas and Reed (2000) and Teresi et al. (1995).

Integrated multimodality MR image processing

Structural MR image processing

The following key processing steps were performed on each brain image volume for estimations of cortical thickness. First, an expectation maximization segmentation (EMS) algorithm including correction for intensity inhomogeneity (Van Leemput et al., 1999a,b) was applied to the T1w image with supplementary T2w image input, to separate skull, scalp, extra-cranial tissue, cerebellum, and brain stem (at the level of the diencephalon) from the rest of brain volume. The remaining brain volume was voxel-wise classified into fractions of cerebral white matter (WM), cortical gray matter (GM), and sulcal cerebrospinal fluid (CSF). The resulting probabilistic tissue density images were visually assessed for performance quality of skull-stripping, bias field correction, and segmentation. If needed, the tissue density images were further manually corrected for inaccurate skull-stripping and tissue probabilities were re-calculated. Based on the tissue density images, each individual's cortical surface was extracted using a cortical reconstruction method using an implicit surface evolution (CRUISE) technique (Han et al., 2004), which was shown to yield an accurate and topologically correct representation that lies at the geometric center of the cortical GM tissue (Tosun et al., 2006). Each resulting cortical surface was represented as a triangle mesh comprising of approximately 300,000 mesh nodes. Typical results from the cortical surface reconstruction are shown in Fig. 1.

Cortical GM thickness estimate

Cortical thickness at each point in the cortical GM tissue mantle was defined as the sum of the distances from this point to the GM/WM and GM/CSF tissue boundaries following a flow field, which guarantees a one-to-one, symmetric, and continuous correspondence between the two tissue boundaries as illustrated in Fig. 2. A flow field with these properties was computed that followed the gradient of the solution of the Laplace's equation with the cortical GM tissue mantle as its domain (Tosun et al., 2006; Yezzi and Prince, 2003). Cortical thickness was estimated in millimeters at 3-D image voxels on the GM tissue mantle. Estimated cortical thickness values were mapped onto the corresponding central cortical surface using trilinear interpolation at each mesh vertex. Cortical mappings of GM tissue thickness for a representative healthy elderly control and a representative AD patient are shown in Fig. 3.

Perfusion-weighted MR image processing

The key processing steps for quantification of rCBF from cASL-MRI were as follows: for each subject, the labeled and unlabeled (reference) images were first rigidly re-aligned and then the resulting mean labeled and reference images were subtracted from each other, yielding raw perfusion-weighted images. This was followed by the normalization of the raw perfusion-weighted images by the overall mean cASL image (i.e., average of mean labeled and mean reference images) as an approximation for arterial water density (Wen-Chau et al., 2009), and for elimination of spurious signal contributions of very high intensity from arterial vessels. The intensity normalization also reduced the intensity inhomogeneity in EPI. The perfusion-weighted signal was then scaled to obtain a measure equivalent to rCBF, according to

$$rCBF \approx PWI \frac{\lambda e^{R_{1\mathrm{app}} T_{\mathrm{d}}}}{2R_{1\mathrm{app}}},$$

where PWI is the intensity normalized perfusion-weighted image, λ is the brain–blood partition coefficient for water (i.e., 0.95 ml/g), $R_{1app}=(R_{1b}+\lambda R_{1t})$ is the apparent relaxation rate of the cASL signal derived from the relaxation in blood R_{1b} and brain tissue R_{1t}, and T_d is the post-labeling delay time for each image slice. The equation is based on a single compartment model of cASL perfusion in which water exchange between capillaries and brain is instantaneous and homogeneous. Note, rCBF is expressed in institutional rather than in absolute units of ml/100 mg/min, because the transit time of the cASL bolus as well as T1 relaxation, which both impact the magnitude of the cASL signal, could not be determined experimentally due to prohibitively long scan times. Therefore, rCBF values may be biased to the extent that transit time and T1 relaxation differ between patients and controls.

We are interested in the blood flow of cerebral GM, which is bounded by CSF and WM tissues. To correct for variations in the cASL signal due to variable coverage of GM, WM and CSF at each voxel, the rCBF image was corrected for the tissue partial volume effects, which requires intra-subject inter-modality spatial alignment establishing a voxel-by-voxel

anatomical correspondence between rCBF image space and structural MR image space where tissue densities (i.e., GM, WM, and CSF) were defined.

One of the key challenges in inter-modality spatial alignment is achieving an accurate anatomical match between EPI-based perfusion images, which suffer from nonlinear geometric distortion due to magnetic susceptibility variations, and structural MR images, which are less susceptible to geometric distortions. We used a fluid-flow warping based distortion correction algorithm, minimizing an image dissimilarity metric between EPI and structural MR image volumes. Specifically, both mean reference image and rCBF image were first mapped onto the T2w structural image space using a multi-resolution affine registration algorithm based on normalized mutual information. The co-registered mean reference image was then fluid-flow warped to the T2w image (Lorenzen et al., 2005). The resulting nonlinear deformation vector field was applied to the affine registered rCBF image. Finally, the T2w image was rigidly aligned to the T1w image for domains with defined tissue densities, cortical geometry, and thickness measures. The T2w to T1w rigid alignment transformation was then applied to the nonlinear geometric distortion corrected rCBF image, yielding an aligned image $rCBF_{CORR}$.

To correct rCBF at each voxel for partial volume variations, two assumptions were made: (1) $rCBF_{CORR}$ is a weighted linear combination of perfusion from GM and WM (i.e., $rCBF_{GM}$ and $rCBF_{WM}$, respectively), with the weighting coefficients expressing perfusion in terms of the corresponding tissue densities (i.e., β_i for i=GM, WM); (2) the relationship between GM and WM perfusion is spatially constant (i.e., $CBF_{GM}=\kappa\times CBF_{WM}$ where $\kappa=2.5$ was used from literature values (Kanetaka et al., 2004)). Accordingly, partial volume correction of $rCBF_{CORR}$ is given by $rCBF_{PVE}=\frac{\beta_{GM}}{\beta_{GM}+\beta_{WM}/\kappa}rCBF_{CORR}$.

Finally, for integrated multimodality data analysis, we generated cortical surface map of $rCBF_{PVE}$ by integrating the $rCBF_{PVE}$ values over a curvilinear line bounded by the GM tissue thickness at every surface mesh node. The curvilinear line was locally defined by the Laplace's equations flow field, which provided the continuous correspondence between the GM/WM and GM/CSF tissue boundaries, as used for local cortical thickness estimations and illustrated in Fig. 2. Representative cortical maps of $rCBF_{PVE}$ for a healthy elderly control and an AD patient are shown in Fig. 3. Note that, the most inferior temporal lobe was not covered with arterial spin labeling MRI, because of technical limitations. Therefore, rCBF values in this region are set to zero and not included in the statistical analysis described in the next section.

Finally, to account for global variations in cerebral blood flow between and within subjects, each subject's average $rCBF_{PVE}$ of the sensorimotor cortex region was obtained (Yakushev et al., 2009) and used as covariate in statistical tests of rCBF effects. The sensorimotor cortex is one of the brain regions known to be largely spared in AD and therefore it is thought that rCBF of this region is unaffected by AD. The sensorimotor cortex was manually labeled in the reference cortical surface and the label was then automatically inherited by the subject cortical surfaces based on the anatomical correspondence established by the cortical spatial normalization between subject's cortical surface and reference cortical surface [cf. Cortical Spatial Normalization].

Surface-based cortical data analysis

Cortical spatial normalization

An image analysis technique known as cortical spatial normalization was used to match anatomically homologous cortical features across subjects before performing cross-subject comparisons. Specifically, the central cortical surface model of each subject was spatially normalized with respect to the geometry of a representative reference brain using an automated surface-based cortical warping method (Tosun and Prince, 2008). Structural brain MRI scan from a healthy female of age 65 years old was selected as the representative reference cortical surface model in this study.

Briefly, the central cortical surfaces were automatically unfolded to a spherical shape using surface partial flattening and conformal mapping with a minimal area distortion constraint (Tosun et al., 2004). Of note, this was done for left and right hemispheres separately, yielding a map of each cortical hemisphere onto its own unit sphere. Left and right cortical hemispheres were automatically identified by defining a surface cut around the corpus callosum using the knowledge of the locations of the anterior and posterior commissures. Anatomical correspondence between mesh nodes on the subject's and the reference brain's hemispheres were established by calculating a geometry-driven optical flow field, which provided a dense representation of the displacement that was required to warp one cortex so that it best matched the other in the spherical coordinate system.

In particular, the algorithm first analyzed the geometry of each central cortical surface in a multi-scale framework. In multi-scale framework, multiple partially flattened surface representations were generated by gradually smoothing the central cortical surface up to pre-defined folding complexity scales, measured by a global shape measure (i.e., surface bending energy) (Tosun et al., 2004). Curvature characteristics representing the type and size of the surface folding (i.e., gross anatomical landmarks) for each partially flattened surface representation were computed. An optical flow warping was formulated to match the curvature characteristics from all scales of the subject to the ones of the reference cortical surface (Tosun and Prince, 2008). Therefore, each subject's cortical surface was spatially normalized with respect to the geometry of the representative reference brain. As a result, individual cortical morphometry measures from homologous surface locations were mapped onto the reference surface, enabling statistical analyses vertex-by-vertex across subjects.

Integrated multimodality MR image analysis

To reduce local variations across subjects due to misregistrations and also to increase the signal-to-noise ratio, a surface-based intrinsic isotropic diffusion kernel was applied to blur the images before performing surface-based statistical tests. Specifically, the estimated value of a cortical feature map (i.e., cortical thickness and $rCBF_{PVE}$) at each surface mesh node was replaced by the convolution of the feature map of interest with a Gaussian kernel centered at this mesh node. The Gaussian kernel domain was defined on each cortical surface over geodesic neighborhoods of radius 10 mm and 8 mm for cortical thickness and $rCBF_{PVE}$ measures, respectively. A 5-to-4 ratio between cortical thickness and $rCBF_{PVE}$ smoothing kernels was estimated on the surface as described in Hagler et al. (2006) to

achieve comparable degrees of smoothing. The size of the smoothing kernel matched the size of the effect we sought while accounting for residual errors in the surface warping. For each subject brain, smoothed measure values at each surface mesh node were transferred onto the anatomically homologous location on the reference brain surface according to the surface correspondence established by the spatial normalization.

Classification of AD and CN

We assessed the contribution of imaging measures to the classification of AD and CN subjects within the GLM framework, using the logit function as link between the linear predictor variables (i.e., cortical thickness and rCBF) and diagnosis as binomial outcome variable (AD=1 versus CN=0). The logistic linear regression analysis allowed to determine the classification power of $rCBF_{PVE}$ and cortical thickness individually as well as when they were used together. In particular, logistic linear regression analysis was used to determine separately the classification power of (a) $rCBF_{PVE}$ alone, (b) cortical thickness alone, as well as (c) $rCBF_{PVE}$, cortical thickness, and their interaction together for a correct classification of AD and controls. In detail, the logistic regression functions to test either $rCBF_{PVE}$ or cortical thickness alone for group classification were a) $\log\frac{Pr(D=AD|i)}{1-Pr(D=AD|i)}\sim\beta_0+\beta_1 P_i+\varepsilon_P$ and b) $\log\frac{Pr(D=AD|i)}{1-Pr(D=AD|i)}\sim\alpha_0+\alpha_1 T_i+\varepsilon_T$, respectively. Similarly, the logistic regression function to test their joint power and interaction was c) $\log\frac{Pr(D=AD|i)}{1-Pr(D=AD|i)}\sim\gamma_0+\gamma_1 P_i+\gamma_2 T_i+\gamma_3 P_i\cdot T_i+\varepsilon_{TP}$. Here $\frac{Pr(D=AD|i)}{1-Pr(D=AD|i)}$ represents the probability of a correct diagnostic classification (AD or controls) given all individuals *i* in the study populations. The α's, β's, γ's are the corresponding regression coefficients, *P* and *T* respectively are $rCBF_{PVE}$ and cortical thickness measurements, and the ε's indicate randomerrors associated with each image modality.

To determine the contribution of each measure to the correct classification of AD and CN given the other measure(s), nested logistic regression models with and without the target measure (i.e., $rCBF_{PVE}$, cortical thickness, or their interaction) were constructed and compared using likelihood ratio tests with a Chi-squared statistic (Hosmer and Lemeshow, 2000). Note, the logistic regression functions were executed point-by-point on the reference cortical surface and the statistic was adjusted for multiple comparisons as described below.

To correct for multiple comparisons, we used permutation testing to assess the overall significance of diagnosis-feature map association. A null distribution for the diagnosis-feature map association at each surface mesh node was constructed using 10,000 random permutations of the data. For each test, the subjects' diagnosis was randomly permuted and point-wise *t*-tests were conducted to identify surface mesh nodes where the null distribution was rejected at the p=0.05 level. Significance maps were computed for both the real experiment with original diagnosis labels and for the permutations. Finally, the number of times the supra-threshold surface area exceeded the original effects surface area in the permutations was counted to yield an overall *p*-value for the significance of the map.

The predicted classification of CN and AD subjects based on logistic linear regression at each surface point were used to fit Receiver Operating Characteristic (ROC) curves point by point on the brain surface. The area under the ROC curves (AUC), and the classification sensitivity and specificity at the level of maximum accuracy at each surface point were calculated. Average AUC, maximum accuracy, sensitivity, and specificity measures were calculated for statistically significant region of interests (sROIs). For structural imaging, sROIs were defined based on surface mesh nodes with significant cortical atrophy (i.e., thinner cortex) at the level $p<0.01$. In particular, the significance map from logistic regression using structural MRI alone as predictor was thresholded at the level $p=0.01$ on the reference cortical surface. The thresholded surface area was then parcellated to single connected regions. Regions with surface area smaller than 100 mm^2 were ignored and the remaining regions were identified as sROIs of structural imaging. Each structural sROI was then mapped back to each subject's cortical surface using the anatomical correspondence established by the cortical spatial normalization. Similarly, perfusion sROIs were identified based on the significance map of logistic regression using $rCBF_{PVE}$ alone as predictor.

Accounting for variance in the severity of cognitive impairment of AD

Our last aim was to determine which brain regions and MRI measures (cortical thinning, rCBF or both together) account for the variability in cognitive impairment, as measured by remapped MMSE scores, termed ability metrics. For this test, average cortical thickness in each structural sROI and average $rCBF_{PVE}$ in each perfusion sROI were computed for each subject. We then linearly regressed the ability metrics against the average cortical thickness and $rCBF_{PVE}$ measurements from each sROI.

In all regression analyses (i.e., logistic and generalized) described above, sex was included as a covariate to account for a potential bias toward different ratios of males and females within each diagnostic group. Age was included as a second covariate to account for age-related variations in $rCBF_{PVE}$ and cortical thickness. Furthermore, in regression analyses with $rCBF_{PVE}$ as a predictor, sensorimotor cortex average $rCBF_{PVE}$ was included as an additional covariate. Group average values of the sensorimotor cortex mean $rCBF_{PVE}$ was 7559.1± 1907.9 ml/100 mg/min in the CN group and 6449.4±1788.4 ml/100 mg/min in the AD group. The sensorimotor cortex mean $rCBF_{PVE}$ was significantly smaller in AD patients than in healthy elderly controls (Student's *t*-test, $p=0.01$). All statistical computations were carried out using the statistical package R (http://www.r-project.org/).

Results

Cortical thinning

Maps of logistic regression coefficients using cortical thickness alone for the correct classification of CN and AD are shown in Fig. 4a. Widespread cortical thinning in the temporo-parietal, middle frontal, superior frontal, posterior cingulate, anterior cingulate, precuneus, cuneus, and entorhinal cortices bilaterally had the best classification power, as indicated in the corresponding significance map corrected at $p=0.05$ in Fig. 4b.

Hypoperfusion

Maps of logistic regression coefficients using $rCBF_{PVE}$ alone for the correct classification of AD and CN are shown in Fig. 5. $rCBF_{PVE}$ reduction in the inferior parietal lobule, superior parietal lobule, superior temporal, middle frontal, precuneus, posterior cingulate, hippocampal gyrus bilaterally had the highest classification power, as indicated in the corresponding significance map illustrated in Fig. 5b. Qualitatively, spatial spread and diagnosis classification power of $rCBF_{PVE}$ reduction was more pronounced in the left than right cortical hemisphere.

Joint contribution of reduced rCBF and cortical thinning

Using cortical thinning and rCBF together for the correct classification of AD and CN showed that rCBF contributions were no longer significant compared to contributions from cortical thinning throughout the brain (Figs. 5a and 6a). The statistical significance of the dominance of cortical thinning over rCBF for the classification was tested by 60-fold boots trapping. As shown in Fig. 7, the dominance of cortical thinning over rCBF for the classification was significant in the right inferior parietal lobule, right superior temporal, right middle frontal, right precuneus, right posterior cingulate, left inferior parietal lobule, left superior parietal, left superior temporal, left precuneus, and left posterior cingulate cortices. rCBF, by contrast, never reached dominance over cortical thinning for the classification in any brain region. Results are shown in Figs. 4a and 6b.

Interaction between reduced rCBF and cortical thinning

The map of logistic regression coefficients using the interaction between regional rCBF and cortical thinning for the correct classification of AD and CN is depicted in Fig. 8, together with the corresponding significance map. A positive interaction (i.e., more $rCBF_{PVE}$ reduction and cortical thinning) was observed in the right superior temporal and right middle temporal cortices and a negative interaction (i.e., less $rCBF_{PVE}$ reduction and cortical thinning) in the left inferior parietal lobule were observed. However, only the positive interaction in the right superior temporal sulcus region reached statistical significance.

Classification accuracy

For each significant structural sROI and perfusion sROI, the average AUC, maximum accuracy and the corresponding sensitivity and specificity values from a classification using either cortical thickness and $rCBF_{PVE}$ alone or both together as predictors are reported in the Supplementary Table 1. For structural sROIs, the classification based on cortical thickness alone increased on average only marginally by less than 1% when rCBF and the interaction between rCBF and cortical thickness were added as predictor variables. For perfusion sROIs, by contrast, accuracy and specificity of the classification based on rCBF alone improved substantially by 9.4% and 15.2% respectively, when cortical thickness and the interaction between rCBF and cortical thickness were added as predictor variables, whereas sensitivity decreased marginally by 1.6%.

Relationship between reduced rCBF, cortical thinning, and severity of cognitive impairment in AD

We further tested the extent to which cortical thinning and cortical rCBF explain separately or together severity of cognitive impairment in AD, as measured using MMSE scores. The R^2 values of the linear regressions with the MRI measures as predictors and the "linearized" MMSE scores as outcome are listed in Table 2 by sROI. Also shown in Table 2 are the corresponding regression coefficients β and standard errors as well as the significance of the regressions. Average cortical thickness from each structural sROI explained between 17 and 54% of the variability in severity of cognitive impairment in AD. Average cortical thickness of left temporal brain regions was the best predictor for MMSE variability. Taking all structural sROIs with significant contributions together as predictor explained 72% of the variability in MMSE.

In contrast to cortical thinning, average $rCBF_{PVE}$ from sROIs explained alone only between 4 and 26% of the variability in MMSE. Taking all perfusion sROIs with significant contributions together explained 47% of the variability in MMSE. Reduced rCBF in left precuneus cortex was the best predictor for MMSE variability.

Taking cortical thickness of each structural sROI and rCBF of each perfusion sROI together in a cumulative regression model explained 75% of the variability in MMSE in AD with statistical significance of $p<10^{-4}$. Based on pair-wise maximum likelihood tests between cumulative models with and without individual sROIs, we found the average cortical thickness of left entorhinal (likelihood ratio=12.0), right cuneus (likelihood ratio=7.1), and right precuneus (likelihood ratio=6.3) cortices were the best predictors for variability in MMSE in AD.

Discussion

The major findings are: (1) separate analyses of structural MRI and cASL-MRI data yielded the well-established pattern of cortical thinning and rCBF reduction in AD, consistent with previous neuroimaging studies, including PET and SPECT. (2) Using measurements from structural MRI and cASL-MRI jointly indicated that cortical thinning dominated the classification of AD and controls without significant diagnostic contributions from rCBF measurements. (3) Considering furthermore the relationship between reduced rCBF and cortical thinning revealed a positive interaction between the two measures in the right superior temporal sulcus. (4) Regional cortical thinning explained variability in MMSE in AD better than reduced rCBF.

We demonstrated that changes in cortical thickness in the temporal, parietal, frontal, cingulate, precuneus, cuneus, and entorhinal cortices are predictive for correct classifications of CN and AD, irrespective of rCBF variations. The pattern is congruent with the well-established literature on structural changes in AD using voxel-based and surface-based cortical morphometry (Apostolova and Thompson, 2008; Calvini et al., 2009; Desikan et al., 2008; Ezekiel et al., 2004; Frisoni et al., 2007; Hua et al., 2008a,b; Jack et al., 2004; Scahill et al., 2002; Thompson et al., 2003). Our first finding of substantial rCBF reduction in the parietal and temporal cortices in AD based on cASL-MRI is consistent with many PET and

SPECT neuroimaging studies reporting reduced cortical glucose metabolism and reduced rCBF, respectively in these regions (Callen et al., 2002; El Fakhri et al., 2003; Hanyu et al., 1997; Herholz et al., 2002; Jagust et al., 1995; Messa et al., 1994). These findings support the effectiveness of the presented surface-based mapping for analysis of rCBF image data. Since the presented method of surface-based rCBF mapping offers technical advantages (Kubota et al., 2006), such as improved anatomical localization of the rCBF signal and intrinsic smoothing of local signal variations, compared to conventional voxel-based methods, the approach holds promise for improved assessment of cASL-MRI data in particular and other image modalities, including PET and SPECT, in general.

Our observation of rCBF deficits in frontal lobe regions in AD is noteworthy, because most functional imaging studies suggest deficits in temporo-parietal regions are more characteristic for AD (Devous, 2002). However, findings of frontal lobe involvement in AD are not uncommon (Bradley et al., 2002) and some SPECT studies even reported diminished rCBF in frontal lobe regions as a prominent feature of AD (Trollor et al., 2005). Because the pathological burden in frontal lobe regions in AD appears to be generally low across the spectrum of disease severity (Claus et al., 1994), it has been argued that the reductions in rCBF in frontal lobe regions represent a “disconnection” of these regions from their rich afferent inputs from parietal limbic regions. Additional studies will be necessary to determine the anatomical relationship between our rCBF finding in the frontal lobe and those in limbic regions. Another explanation for reduced rCBF in frontal lobe regions in AD is comorbidity of psychiatric conditions, especially depression (Hirono et al., 1998; Levy-Cooperman et al., 2008). Four AD patients had a clinical depression diagnosis and 1 AD patient self-reported a history of depression; the number of subjects with depression in our study was too small to determine reliably whether rCBF reduction in the frontal lobe was primarily driven by the AD patients with depression.

Our second finding from a joint analysis of cortical thickness and rCBF implies that measures of cortical thinning largely govern the correct classification of AD and CN while contributions of rCBF measurement to the classification are no longer relevant once cortical thickness is taken into account. One interpretation of this result is that rCBF is diminished proportionately to brain tissue loss and therefore provides little additional information to structural alterations.

Although the current results do not show any significant added value of rCBF to measurements of cortical thinning for the classification of AD from controls, this should not be interpreted that rCBF measurements have no value in the study of AD. For example, rCBF measurements may demonstrate different correlations with various measures of cognitive, behavioral, or emotional functions in AD patients. rCBF may provide additional information concerning change in the brain in early stages of AD, such as MCI, or the effects of ApoE ε4, or in completely normal subjects who are at high risk for AD. For example, a pattern classification study based on joint evaluation of PET and structural imaging in MCI patients reported 98% diagnostic classification, an almost complete match with clinical accuracy, while 87% accuracy was achieved with MRI data alone and only a 50% classification accuracy was obtained with PET data alone without the joint evaluation (Fan et al., 2008). Studies by Reiman et al. (2005) suggest that FDG PET detects changes in

the brains of ApoE ε4 subjects with little or minimal structural change. rCBF may detect similar changes to those detected by FDG PET. Furthermore, ASL-MRI studies recently reported elevated rCBF in presence of atrophy in MCI (Dai et al., 2009) and even in mild AD (Alsop et al., 2008).

Our third finding of a positive interaction between reduced rCBF and cortical thinning involved the right superior temporal sulcus, a major anatomical substrate for selective attention (Cabeza and Nyberg, 2000). Although the biological underpinning of a detrimental interaction between cortical thinning and rCBF reduction remains unclear, there are several possible interpretations for this finding. First, reduced rCBF could be the consequence of dendritic arborizations that further leads to massive cortical neurodegeneration and gray matter loss. A second possibility is that AD pathology includes a vascular component, possibly causing an rCBF reduction because of limited blood supply, which leads secondarily to cortical atrophy (Bidzan, 2005; Cacabelos et al., 2003; Claassen and Jansen, 2006). Our study is the first, to our knowledge, to investigate synergistic effects of reduced rCBF and cortical thinning point-by-point from a joint analysis of structural and cASL-MRI data. However, the sequence of events that leads to reduced rCBF and cortical thinning and the implications for a better understanding of concurrent structural and physiological alterations in AD remains to be determined. Finally, we showed that compared to reduced rCBF, regional cortical thinning better explained the variability in dementia severity, as measured using MMSE. Average cortical thickness of left temporal brain region was the best predictor for MMSE variability in AD. However, the current analysis did not examine specific cognitive functions, only the global measure of MMSE. Nonetheless, the left temporal cortex plays a major role in speech, language, and communication skills (Cabeza and Nyberg, 2000) and impaired communicative functions in AD, partially related to poor memory functions, is well documented (Bayles, 1991). In contrast to cortical thinning, reduced rCBF of the left precuneus cortex was the best explanatory measure among all rCBF-sROIs for MMSE scores in AD. The precuneus is implicated in the recollection of past episodes (Cabeza and Nyberg, 2000) and cognitive decline in episodic memory is one of the earliest clinical syndromes of AD. Reduced rCBF in the left precuneus could therefore be an early marker of AD. From all sROIs of prominent cortical thinning and rCBF reductions that explained variability in MMSE in AD, the left entorhinal, right cuneus, and right precuneus cortices were the best predictors. These regions play a major role in procedural, working, and episodic memory as well as attention. The findings are consistent with the concept that cortical thinning in temporal and parietal regions represents AD pathology and therefore might be an imaging marker for prediction and progression of AD. However, additional analyses are warranted to elucidate the relationships between specific cognitive domains and cortical thinning or reduced rCBF.

Our joint analysis of structural and cASL-MRI data was based on general linear models (GLM). For GLM, it is well known that collinearity among the predictor variables can inflate the variance of parameter estimations. Minimizing the collinearity is not straightforward, especially in the context of multimodal imaging when relationships between variables can vary from region to region. In another study of joint structural and cASL-MRI analysis in AD (Hayasaka et al., 2006), which used non-parametric correlation tests, we showed that structural and rCBF alterations can be intrinsically concordant with each other

in some brain regions while they can be largely discordant in other regions. Hence, it is possible that the accuracy of parameter estimations in our study based on GLM could be regionally biased as a function of regionally variable collinearity between structural and rCBF measures. Several approaches of joint multimodal image analysis are emerging that are not based on GLM. For example, joint independent components analysis (jICA), which tries to combine all heterogeneous information from multimodal imaging in a huge input space, has recently been proposed for the identification of principle interactions across multimodal measurements (Calhoun et al., 2006). At the other end of the spectrum are naïve Bayesian methods, which aim breaking the multimodality problem into subclasses with posterior probabilities for each image modality and using the rules of probability to systematically combine the classes (Daunizeau et al., 2007). Additional studies are warranted to elucidate the effectiveness of the different concepts to jointly analyze multimodal imaging data.

Several other limitations of the study should be mentioned. First, it has been shown that rCBF measurements with cASL-MRI are sensitive to the setting of acquisition parameters due to age-related variations in physiological conditions. In particular, age was associated with changes in relaxation times of blood water (Cho et al., 1997) and prolonged arterial transit time was observed in AD patients (Hunter et al., 1989). Therefore, we cannot rule out that some variations in rCBF could simply be measurement artifacts that are unrelated to differences in brain function between AD patients and controls. In integrated multimodality MR image processing, the accuracy of the intra-subject inter-modality co-registration is limited since cASL-MRI is more prone to geometric distortion and imaging artifacts compared to structural MRI. The partial volume correction and anatomical localization in rCBF measure is also limited by the differences in point spread function of structural and cASL MRIs. In addition, cortical spatial normalization accuracy and consequently accurate partial volume correction might be compromised in AD as a result of averaging across dissimilar structures. Thus, changes in gyralmorphology may have biased rCBF measurements. Taken together, errors in image registration and localization may have diminished power to detect intrinsic relationships between structural and physiological alterations in AD at a local level. Another study limitation that should be mentioned is the cross-sectional design of the statistical analyses reported, which does not permit establishing causality between structural and perfusion alterations. Longitudinal studies will be necessary to further understand the synergistic effects of anatomical and perfusion changes in AD. A conceptual limitation relates to the selection of a surface-based analysis to study the cortical thickness and rCBF jointly. Although, surface-based registration provides generally better spatial normalization of cortical data, the price one pays is the restriction of the analysis to cortical regions. In contrast, a voxel-based approach provides insight into subcortical atrophy and blood flow, but generally at the expense of less accurate cortical registrations. Another conceptual limitation relates to the dense analysis of cortical data, which requires correction for multiple comparisons. Compared to a region-of-interest- based analysis, a point-by-point analysis followed by multiple comparison correction suffers greater loss of statistical power. From a clinical research point of view, another limitation is that all the analysis presented in this study relies on the clinical diagnosis of probable AD without confirmation by autopsy. A clinical diagnosis of AD, even at specialized centers has

typically an accuracy rate of about 90% or lower using the established consensus criteria for probable AD. Therefore, our classification results remain inconclusive to the extent that about 10% of the patients may have been misclassified. Finally, MMSE scores provide a global assessment of cognitive function but no detailed information about deficits in specific cognitive domains. Additional analyses involving comprehensive neurocognitive and neurobehavioral test data are necessary to better understand the extent to which joint brain structural and rCBF alterations explain the variability in cognitive disabilities in AD.

In summary, we presented an integrated multimodality image processing and analysis framework for joint assessments of regional variations in cortical thinning and rCBF that included a point-by-point cortical surface-based analysis and non-parametric tests by permutations. We found that cortical thinning largely dominated the classification of AD and controls and also better explained the variability in dementia severity than rCBF. However, we also found synergistic interactions between cortical thinning and rCBF reductions in some brain regions, supporting the value of joint analysis of structural and perfusion imaging data in AD and normal aging.

Supplementary Material

Refer to Web version on PubMed Central for supplementary material.

Acknowledgments

This work was supported by the National Institutes of Health grant P41 RR23953 and the Department of Defense grant W81XWH-05-2- 0094. This work has also been made possible by use of research facilities at the Veterans Affairs Medical Center in San Francisco.

References

Alsop DC, Casement M, de Bazelaire C, Fong T, Press DZ. Hippocampal hyperperfusion in Alzheimer's disease. NeuroImage. 2008; 42:1267–1274. [PubMed: 18602481]

Anticevic A, Dierker DL, Gillespie SK, Repovs G, Csernansky JG, Van Essen DC, Barch DM. Comparing surface-based and volume-based analyses of functional neuroimaging data in patients with schizophrenia. NeuroImage. 2008; 41:835–848. [PubMed: 18434199]

Apostolova LG, Thompson PM. Mapping progressive brain structural changes in early Alzheimer's disease and mild cognitive impairment. Neuropsychologia. 2008; 46:1597–1612. [PubMed: 18395760]

Arbizu J, Larumbe R, Rubio L, Villas A, Martinez-Lage JM, Richter JA. Cerebral SPECT and neuropsychological function in Alzheimer's disease. Rev Med Univ Navarra. 1997; 41:12–18. [PubMed: 9527710]

Asllani I, Habeck C, Scarmeas N, Borogovac A, Brown TR, Stern Y. Multivariate and univariate analysis of continuous arterial spin labeling perfusion MRI in Alzheimer's disease. J Cereb Blood Flow Metab. 2008; 28:725–736. [PubMed: 17960142]

Basso M, Yang J, Warren L, MacAvoy MG, Varma P, Bronen RA, van Dyck CH. Volumetry of amygdala and hippocampus and memory performance in Alzheimer's disease. Psychiatry Res: Neuroimaging. 2006; 146:251–261. [PubMed: 16524704]

Bayles KA. Alzheimer's disease symptoms: prevalence and order of appearance. J Appl Gerontol. 1991; 10:419–430.

Benoit M, Dygai I, Migneco O, Robert PH, Bertogliati C, Darcourt J, Benoliel J, Aubin-Brunet V, Pringuey D. Behavioral and psychological symptoms in Alzheimer's disease. Relation between

apathy and regional cerebral perfusion. Dement Geriatr Cogn Disord. 1999; 10:511–517. [PubMed: 10559568]

Bidzan L. Vascular factors in dementia. Psychiatr Pol. 2005; 39:977–986. [PubMed: 16358596]

Braak H, Braak E. Neuropathological stageing of Alzheimer-related changes. Acta Neuropathol. 1991; 82:239–259. [PubMed: 1759558]

Bradley KM, O'Sullivan VT, Soper ND, Nagy Z, King EM, Smith AD, Shepstone BJ. Cerebral perfusion SPET correlated with Braak pathological stage in Alzheimer's disease. Brain. 2002; 125:1772–1781. [PubMed: 12135968]

Bruen PD, McGeown WJ, Shanks MF, Venneri A. Neuroanatomical correlates of neuropsychiatric symptoms in Alzheimer's disease. Brain. 2008; 131:2455–2463. [PubMed: 18669506]

Cabeza R, Nyberg L. Imaging cognition II: an empirical review of 275 PET and fMRI studies. J Cogn Neurosci. 2000; 12:1–47. [PubMed: 10769304]

Cacabelos R, Fernandez-Novoa L, Lombardi V, Corzo L, Pichel V, Kubota Y. Cerebrovascular risk factors in Alzheimer's disease: brain hemodynamics and pharmacogenomic implications. Neurol Res. 2003; 25:567–580. [PubMed: 14503010]

Calhoun VD, Adali T, Giuliani NR, Pekar JJ, Kiehl KA, Pearlson GD. Method for multimodal analysis of independent source differences in schizophrenia: combining gray matter structural and auditory oddball functional data. Hum Brain Mapp. 2006; 27:47–62. [PubMed: 16108017]

Callen DJ, Black SE, Caldwell CB. Limbic system perfusion in Alzheimer's disease measured by MRI-coregistered HMPAO SPET. Eur J Nucl Med Mol Imaging. 2002; 29:899–906. [PubMed: 12111130]

Calvini P, Chincarini A, Gemme G, Penco MA, Squarcia S, Nobili F, Rodriguez G, Bellotti R, Catanzariti E, Cerello P, De Mitri I, Fantacci ME. Automatic analysis of medial temporal lobe atrophy from structural MRIs for the early assessment of Alzheimer disease. Med Phys. 2009; 36:3737–3747. [PubMed: 19746807]

Chetelat GA, Baron JC. Early diagnosis of Alzheimer's disease: contribution of structural neuroimaging. NeuroImage. 2003; 18:525–541. [PubMed: 12595205]

Cho S, Jones D, Reddick WE, Ogg RJ, Steen RG. Establishing norms for age-related changes in proton T1 of human brain tissue in vivo. Magnetic Resonance Imaging. 1997; 15:1133–1143. [PubMed: 9408134]

Claassen JA, Jansen RW. Cholinergically mediated augmentation of cerebral perfusion in Alzheimer's disease and related cognitive disorders: the cholinergic-vascular hypothesis. J Gerontol A Biol Sci Med Sci. 2006; 61:267–271. [PubMed: 16567376]

Claus JJ, Harskamp FV, Breteler MMB, Krenning EP, Koning ID, van der Cammen TJM, Hofman A, Hasan D. The diagnostic value of SPECT with Tc 99m HMPAO in Alzheimer's disease: a population-based study. Neurology. 1994; 44:454. [PubMed: 8145915]

Dai W, Lopez OL, Carmichael OT, Becker JT, Kuller LH, Gach HM. Mild cognitive impairment and Alzheimer disease: patterns of altered cerebral blood flow at MR imaging. Radiology. 2009; 250:856–866. [PubMed: 19164119]

Daunizeau J, Grova C, Marrelec G, Mattout J, Jbabdi S, Pélégrini-Issac M, Lina JM, Benali H. Symmetrical event-related EEG/fMRI information fusion in a variational Bayesian framework. NeuroImage. 2007; 36:69–87. [PubMed: 17408972]

Desikan RS, Fischl B, Cabral HJ, Kemper TL, Guttmann CRG, Blacker D, Hyman BT, Albert MS, Killiany RJ. MRI measures of temporoparietal regions show differential rates of atrophy during prodromal AD. Neurology. 2008; 71:819–825. [PubMed: 18672473]

deToledo-Morrell L, Stoub TR, Bulgakova M, Wilson RS, Bennett DA, Leurgans S, Wuu J, Turner DA. MRI-derived entorhinal volume is a good predictor of conversion from MCI to AD. Neurobiol Aging. 2004; 25:1197–1203. [PubMed: 15312965]

Detre JA, Alsop DC. Perfusion magnetic resonance imaging with continuous arterial spin labeling: methods and clinical applications in the central nervous system. Eur J Radiol. 1999; 30:115–124. [PubMed: 10401592]

Detre JA, Leigh JS, Williams DS, Koretsky AP. Perfusion imaging. Magn Reson Med. 1992; 23:37–45. [PubMed: 1734182]

Devous M. Functional brain imaging in the dementias: role in early detection, differential diagnosis, and longitudinal studies. Eur J Nucl Med Mol Imaging. 2002; 29:1685–1696. [PubMed: 12458405]

Du AT, Jahng GH, Hayasaka S, Kramer JH, Rosen HJ, Gorno-Tempini ML, Rankin KP, Miller BL, Weiner MW, Schuff N. Hypoperfusion in frontotemporal dementia and Alzheimer disease by arterial spin labeling MRI. Neurology. 2006; 67:1215–1220. [PubMed: 17030755]

El Fakhri G, Kijewski MF, Johnson KA, Syrkin G, Killiany RJ, Becker JA, Zimmerman RE, Albert MS. MRI-guided SPECT perfusion measures and volumetric MRI in prodromal Alzheimer disease. Arch Neurol. 2003; 60:1066–1072. [PubMed: 12925361]

Ezekiel F, Chao L, Kornak J, Du AT, Cardenas V, Truran D, Jagust W, Chui H, Miller B, Yaffe K, Schuff N, Weiner M. Comparisons between global and focal brain atrophy rates in normal aging and Alzheimer disease: boundary shift integral versus tracing of the entorhinal cortex and hippocampus. Alzheimer Dis Assoc Disord. 2004; 18:196–201. [PubMed: 15592130]

Fan Y, Resnick SM, Wu X, Davatzikos C. Structural and functional biomarkers of prodromal Alzheimer's disease: a high-dimensional pattern classification study. NeuroImage. 2008; 41:277–285. [PubMed: 18400519]

Folstein MF, Folstein SE, McHugh PR. "Mini-mental state": a practical method for grading the cognitive state of patients for the clinician. J Psychiatr Res. 1975; 12:189–198. [PubMed: 1202204]

Frisoni GB, Pievani M, Testa C, Sabattoli F, Bresciani L, Bonetti M, Beltramello A, Hayashi KM, Toga AW, Thompson PM. The topography of grey matter involvement in early and late onset Alzheimer's disease. Brain. 2007; 130:720–730. [PubMed: 17293358]

Gilboa A, Ramirez J, Köhler S, Westmacott R, Black SE, Moscovitch M. Retrieval of autobiographical memory in Alzheimer's disease: relation to volumes of medial temporal lobe and other structures. Hippocampus. 2005; 15:535–550. [PubMed: 15884035]

Hagler DJ, Saygin AP, Sereno MI. Smoothing and cluster thresholding for cortical surface-based group analysis of fMRI data. NeuroImage. 2006; 33:1093–1103. [PubMed: 17011792]

Han X, Pham DL, Tosun D, Rettmann ME, Xu C, Prince JL. CRUISE: cortical reconstruction using implicit surface evolution. NeuroImage. 2004; 23:997–1012. [PubMed: 15528100]

Hanyu H, Asano T, Abe S, Arai H, Takasaki M, Shindo H, Abe K. Single photon emission computed tomography in the diagnosis of Alzheimer's disease. Nippon Ronen Igakkai Zasshi. 1997; 34:468–473. [PubMed: 9301261]

Hashikawa K, Matsumoto M, Moriwaki H, Oku N, Okazaki Y, Seike Y, Uehara T, Tanabe H, Ohie Y, Kamada T, et al. Three-dimensional display of surface cortical perfusion by SPECT: application in assessing Alzheimer's disease. J Nucl Med. 1995; 36:690–696. [PubMed: 7699466]

Hayasaka S, Du AT, Duarte A, Kornak J, Jahng GH, Weiner MW, Schuff N. A non-parametric approach for co-analysis of multi-modal brain imaging data: application to Alzheimer's disease. NeuroImage. 2006; 30:768–779. [PubMed: 16412666]

Herholz K, Schopphoff H, Schmidt M, Mielke R, Eschner W, Scheidhauer K, Schicha H, Heiss WD, Ebmeier K. Direct comparison of spatially normalized PET and SPECT scans in Alzheimer's disease. J Nucl Med. 2002; 43:21–26. [PubMed: 11801698]

Hirono N, Mori E, Ishii K, Ikejiri Y, Imamura T, Shimomura T, Hashimoto M, Yamashita H, Sasaki M. Frontal lobe hypometabolism and depression in Alzheimer's disease. Neurology. 1998; 50:380–383. [PubMed: 9484357]

Hosmer, DW.; Lemeshow, S. Applied logistic regression. 2. John Wiley and Sons; 2000. illustrated ed

Hua X, Leow AD, Lee S, Klunder AD, Toga AW, Lepore N, Chou YY, Brun C, Chiang MC, Barysheva M, Jack CR, Bernstein MA, Britson PJ, Ward CP, Whitwell JL, Borowski B, Fleisher AS, Fox NC, Boyes RG, Barnes J, Harvey D, Kornak J, Schuff N, Boreta L, Alexander GE, Weiner MW, Thompson PM. the Alzheimer's Disease Neuroimaging I. 3D characterization of brain atrophy in Alzheimer's disease and mild cognitive impairment using tensor-based morphometry. NeuroImage. 2008a; 41:19–34. [PubMed: 18378167]

Hua X, Leow AD, Parikshak N, Lee S, Chiang MC, Toga AW, Jack CR Jr, Weiner MW, Thompson PM. Tensor-based morphometry as a neuroimaging biomarker for Alzheimer's disease: an MRI

study of 676 AD, MCI, and normal subjects. NeuroImage. 2008b; 43:458–469. [PubMed: 18691658]

Hunter R, Merrick M, Ferrington C, Notghi A, McLuskie R, Christie J, Goodwin G. Cerebral vascular transit time in Alzheimer's disease and Korsakoff's psychosis and its relation to cognitive function. Br J Psychiatry. 1989; 154:790–796. [PubMed: 2557110]

Ishii K, Kitagaki H, Kono M, Mori E. Decreased medial temporal oxygen metabolism in Alzheimer's disease shown by PET. J Nucl Med. 1996; 37:1159–1165. [PubMed: 8965188]

Jack CR Jr, Shiung MM, Gunter JL, O'Brien PC, Weigand SD, Knopman DS, Boeve BF, Ivnik RJ, Smith GE, Cha RH, Tangalos EG, Petersen RC. Comparison of different MRI brain atrophy rate measures with clinical disease progression in AD. Neurology. 2004; 62:591–600. [PubMed: 14981176]

Jagust W. Positron emission tomography and magnetic resonance imaging in the diagnosis and prediction of dementia. Alzheimer's Dement. 2006; 2:36–42. [PubMed: 19595854]

Jagust WJ, Johnson KA, Holman BL. SPECT perfusion imaging in the diagnosis of dementia. J Neuroimaging. 1995; 5 (Suppl 1):S45–S52. [PubMed: 7626837]

Jagust WJ, Reed BR, Seab JP, Kramer JH, Budinger TF. Clinical-physiologic correlates of Alzheimer's disease and frontal lobe dementia. Am J Physiol Imaging. 1989; 4:89–96. [PubMed: 2789844]

Johnson NA, Jahng GH, Weiner MW, Miller BL, Chui HC, Jagust WJ, Gorno-Tempini ML, Schuff N. Pattern of cerebral hypoperfusion in Alzheimer disease and mild cognitive impairment measured with arterial spin-labeling MR imaging: initial experience. Radiology. 2005; 234:851–859. [PubMed: 15734937]

Kanetaka H, Matsuda H, Asada T, Ohnishi T, Yamashita F, Imabayashi E, Tanaka F, Nakano S, Takasaki M. Effects of partial volume correction on discrimination between very early Alzheimer's dementia and controls using brain perfusion SPECT. Eur J Nucl Med Mol Imaging. 2004; 31:975–980. [PubMed: 14991240]

Kawachi T, Ishii K, Sakamoto S, Sasaki M, Mori T, Yamashita F, Matsuda H, Mori E. Comparison of the diagnostic performance of FDG-PET and VBM-MRI in very mild Alzheimer's disease. Eur J Nucl Med Mol Imaging. 2006; 33:801–809. [PubMed: 16550383]

Keilp JG, Alexander GE, Stern Y, Prohovnik I. Inferior parietal perfusion, lateralization, and neuropsychological dysfunction in Alzheimer's disease. Brain Cogn. 1996; 32:365–383. [PubMed: 8975677]

Kobayashi S, Tateno M, Utsumi K, Takahashi A, Saitoh M, Morii H, Fujii K, Teraoka M. Quantitative analysis of brain perfusion SPECT in Alzheimer's disease using a fully automated regional cerebral blood flow quantification software, 3DSRT. J Neurol Sci. 2008; 264:27–33. [PubMed: 17764699]

Kubota T, Ushijima Y, Okuyama C, Nishimura T. A region-of-interest template for three-dimensional stereotactic surface projection images: initial application to the analysis of Alzheimer's disease and mild cognitive impairment. Nucl Med Commun. 2006; 27:37–44. [PubMed: 16340722]

Lampl Y, Sadeh M, Laker O, Lorberboym M. Correlation of neuropsychological evaluation and SPECT imaging in patients with Alzheimer's disease. Int J Geriatr Psychiatry. 2003; 18:288–291. [PubMed: 12673603]

Leube DT, Weis S, Freymann K, Erb M, Jessen F, Heun R, Grodd W, Kircher TT. Neural correlates of verbal episodic memory in patients with MCI and Alzheimer's disease—a VBM study. Int J Geriatr Psychiatry. 2008; 23:1114–1118. [PubMed: 18449954]

Levy-Cooperman N, Burhan AM, Rafi-Tari S, Kusano M, Ramirez J, Caldwell C, Black SE. Frontal lobe hypoperfusion and depressive symptoms in Alzheimer disease. J Psychiatry Neurosci. 2008; 33:218–226. [PubMed: 18592038]

Lorenzen P, Davis B, Joshi S. Unbiased atlas formation via large deformations metric mapping. Med Image Comput Comput Assist Interv Int Conf Med Image Comput Comput Assist Interv. 2005:411–418.

Maestu F, Arrazola J, Fernandez A, Simos PG, Amo C, Gil-Gregorio P, Fernandez S, Papanicolaou A, Ortiz T. Do cognitive patterns of brain magnetic activity correlate with hippocampal atrophy in Alzheimer's disease? J Neurol Neurosurg Psychiatry. 2003; 74:208–212. [PubMed: 12531952]

Matsunari I, Samuraki M, Chen WP, Yanase D, Takeda N, Ono K, Yoshita M, Matsuda H, Yamada M, Kinuya S. Comparison of 18F-FDG PET and optimized voxel-based morphometry for detection of Alzheimer's disease: aging effect on diagnostic performance. J Nucl Med. 2007; 48:1961–1970. [PubMed: 18006622]

Messa C, Perani D, Lucignani G, Zenorini A, Zito F, Rizzo G, Grassi F, Del Sole A, Franceschi M, Gilardi MC, et al. High-resolution technetium-99m-HMPAO SPECT in patients with probable Alzheimer's disease: comparison with fluorine-18- FDG PET. J Nucl Med. 1994; 35:210–216. [PubMed: 8294987]

Morra JH, Tu Z, Apostolova LG, Green AE, Avedissian C, Madsen SK, Parikshak N, Hua X, Toga AW, Jack CR Jr, Weiner MW, Thompson PM. Validation of a fully automated 3D hippocampal segmentation method using subjects with Alzheimer's disease mild cognitive impairment, and elderly controls. NeuroImage. 2008; 43:59–68. [PubMed: 18675918]

Morra JH, Tu Z, Apostolova LG, Green AE, Avedissian C, Madsen SK, Parikshak N, Hua X, Toga AW Jr, CRJ, Schuff N, Weiner MW, Thompson PM. Initiative a.t.A.s.D.N. Automated 3D mapping of hippocampal atrophy and its clinical correlates in 400 subjects with Alzheimer's disease, mild cognitive impairment, and elderly controls. Hum Brain Mapp. 2009a; 30:2766–2788. [PubMed: 19172649]

Morra JH, Tu Z, Apostolova LG, Green AE, Avedissian C, Madsen SK, Parikshak N, Toga AW, Jack CR Jr, Schuff N, Weiner MW, Thompson PM. Automated mapping of hippocampal atrophy in 1-year repeat MRI data from 490 subjects with Alzheimer's disease, mild cognitive impairment, and elderly controls. NeuroImage. 2009b; 45:S3–S15. [PubMed: 19041724]

Mosconi L, Tsui WH, De Santi S, Li J, Rusinek H, Convit A, Li Y, Boppana M, de Leon MJ. Reduced hippocampal metabolism in MCI and AD: automated FDG-PET image analysis. Neurology. 2005; 64:1860–1867. [PubMed: 15955934]

Mungas D, Harvey D, Reed BR, Jagust WJ, DeCarli C, Beckett L, Mack WJ, Kramer JH, Weiner MW, Schuff N, Chui HC. Longitudinal volumetric MRI change and rate of cognitive decline. Neurology. 2005; 65:565–571. [PubMed: 16116117]

Mungas D, Reed BR. Application of item response theory for development of a global functioning measure of dementia with linear measurement properties. Stat Med. 2000; 19:1631–1644. [PubMed: 10844724]

Nebu A, Ikeda M, Fukuhara R, Komori K, Maki N, Hokoishi K, Shigenobu K, Kikuchi T, Tanabe H. Utility of (99m)Tc-HM-PAO SPECT hippocampal image to diagnose early stages of Alzheimer's disease using semiquantitative analysis. Dement Geriatr Cogn Disord. 2001; 12:153–157. [PubMed: 11173889]

Nobili F, Brugnolo A, Calvini P, Copello F, De Leo C, Girtler N, Morbelli S, Piccardo A, Vitali P, Rodriguez G. Resting SPECT-neuropsychology correlation in very mild Alzheimer's disease. Clin Neurophysiol. 2005; 116:364–375. [PubMed: 15661114]

Nobili F, Koulibaly PM, Rodriguez G, Benoit M, Girtler N, Robert PH, Brugnolo A, Darcourt J. 99mTc-HMPAO and 99mTc-ECD brain uptake correlates of verbal memory in Alzheimer's disease. Q J Nucl Med Mol Imaging. 2007; 51:357–363. [PubMed: 17220817]

O'Brien JT, Eagger S, Syed GM, Sahakian BJ, Levy R. A study of regional cerebral blood flow and cognitive performance in Alzheimer's disease. J Neurol Neurosurg Psychiatry. 1992; 55:1182–1187. [PubMed: 1479398]

Reed BR, Jagust WJ, Seab JP, Ober BA. Memory and regional cerebral blood flow in mildly symptomatic Alzheimer's disease. Neurology. 1989; 39:1537–1539. [PubMed: 2812339]

Reiman EM, Chen K, Alexander GE, Caselli RJ, Bandy D, Osborne D, Saunders AM, Hardy J. Correlations between apolipoprotein E ε4 gene dose and brain-imaging measurements of regional hypometabolism. Proc Natl Acad Sci USA. 2005; 102:8299–8302. [PubMed: 15932949]

Rémy F, Mirrashed F, Campbell B, Richter W. Verbal episodic memory impairment in Alzheimer's disease: a combined structural and functional MRI study. NeuroImage. 2005; 25:253–266. [PubMed: 15734360]

Rodriguez G, Nobili F, Copello F, Vitali P, Gianelli MV, Taddei G, Catsafados E, Mariani G. 99mTc-HMPAO regional cerebral blood flow and quantitative electroencephalography in Alzheimer's disease: a correlative study. J Nucl Med. 1999; 40:522–529. [PubMed: 10210209]

Rodriguez G, Vitali P, Calvini P, Bordoni C, Girtler N, Taddei G, Mariani G, Nobili F. Hippocampal perfusion inmild Alzheimer's disease. Psychiatry Res. 2000; 100:65–74. [PubMed: 11114492]

Sabbagh MN, Lynn P, Jhingran S, Massman P, Villanueva-Meyer J, Olup J, Doody RS. Correlations between SPECT regional cerebral blood flow and psychometric testing in patients with Alzheimer's disease. J Neuropsychiatry Clin Neurosci. 1997; 9:68–74. [PubMed: 9017531]

Scahill RI, Schott JM, Stevens JM, Rossor MN, Fox NC. Mapping the evolution of regional atrophy in Alzheimer's disease: unbiased analysis of fluid-registered serial MRI. Proc Natl Acad Sci USA. 2002; 99:4703–4707. [PubMed: 11930016]

Schroeter ML, Stein T, Maslowski N, Neumann J. Neural correlates of Alzheimer's disease and mild cognitive impairment: a systematic and quantitative meta-analysis involving 1351 patients. NeuroImage. 2009; 47:1196–1206. [PubMed: 19463961]

Schwartz RS, Burke C, Snars J, Gordon E, Batchelor J, Kostalas G, Meares R, Yiannikas C. Regional cerebral blood flow and recognition memory in elderly normals: potential application to Alzheimer's disease. Clin Exp Neurol. 1991; 28:56–65. [PubMed: 1821840]

Stoub TR, Bulgakova M, Leurgans S, Bennett DA, Fleischman D, Turner DA, deToledo-Morrell L. MRI predictors of risk of incident Alzheimer disease: a longitudinal study. Neurology. 2005; 64:1520–1524. [PubMed: 15883311]

Teresi JA, Golden RR, Cross P, Gurland B, Kleinman M, Wilder D. Item bias in cognitive screening measures: comparisons of elderly white, Afro-American, Hispanic and high and low education subgroups. J Clin Epidemiol. 1995; 48:473–483. [PubMed: 7722601]

Thompson PM, Hayashi KM, de Zubicaray G, Janke AL, Rose SE, Semple J, Herman D, Hong MS, Dittmer SS, Doddrell DM, Toga AW. Dynamics of gray matter loss in Alzheimer's disease. J Neurosci. 2003; 23:994–1005. [PubMed: 12574429]

Thompson PM, Hayashi KM, de Zubicaray GI, Janke AL, Rose SE, Semple J, Hong MS, Herman DH, Gravano D, Doddrell DM, Toga AW. Mapping hippocampal andventricular change in Alzheimer disease. NeuroImage. 2004; 22:1754–1766. [PubMed: 15275931]

Tosun D, Prince JL. A geometry-driven optical flow warping for spatial normalization of cortical surfaces. Med Imaging, IEEE Trans. 2008; 27:1739–1753.

Tosun D, Rettmann ME, Naiman DQ, Resnick SM, Kraut MA, Prince JL. Cortical reconstruction using implicit surface evolution: accuracy and precision analysis. NeuroImage. 2006; 29:838–852. [PubMed: 16269250]

Tosun D, Rettmann ME, Prince JL. Mapping techniques for aligning sulci across multiple brains. Med Image Anal. 2004; 8:295–309. [PubMed: 15450224]

Trollor JN, Sachdev PS, Haindl W, Brodaty H, Wen W, Walker BM. Regional cerebral blood flow deficits in mild Alzheimer's disease using high resolution single photon emission computerized tomography. Psychiatry Clin Neurosci. 2005; 59:280–290. [PubMed: 15896221]

Van Leemput K, Maes F, Vandermeulen D, Suetens P. Automated model-based bias field correction of MR images of the brain. Med Imaging, IEEE Trans. 1999a; 18:885–896.

Van Leemput K, Maes F, Vandermeulen D, Suetens P. Automated model-based tissue classification of MR images of the brain. Med Imaging, IEEE Trans. 1999b; 18:897–908.

Warkentin S, Ohlsson M, Wollmer P, Edenbrandt L, Minthon L. Regional cerebral blood flow in Alzheimer's disease: classification and analysis of heterogeneity. Dement Geriatr Cogn Disord. 2004; 17:207–214. [PubMed: 14739546]

Wen-Chau W, Edlow BL, Elliot MA, Jiongjiong W, Detre JA. Physiological modulations in arterial spin labeling perfusion magnetic resonance imaging. Med Imaging, IEEE Trans. 2009; 28:703–709.

Whitwell JL, Przybelski SA, Weigand SD, Knopman DS, Boeve BF, Petersen RC, Jack CR Jr. 3D maps from multiple MRI illustrate changing atrophy patterns as subjects progress from mild cognitive impairment to Alzheimer's disease. Brain. 2007; 130:1777–1786. [PubMed: 17533169]

Whitwell JL, Shiung MM, Przybelski SA, Weigand SD, Knopman DS, Boeve BF, Petersen RC, Jack CR Jr. MRI patterns of atrophy associated with progression to AD in amnestic mild cognitive impairment. Neurology. 2008; 70:512–520. [PubMed: 17898323]

Wolfe N, Reed BR, Eberling JL, Jagust WJ. Temporal lobe perfusion on single photon emission computed tomography predicts the rate of cognitive decline in Alzheimer's disease. Arch Neurol. 1995; 52:257–262. [PubMed: 7872878]

Yakushev I, Hammers A, Fellgiebel A, Schmidtmann I, Scheurich A, Buchholz HG, Peters JR, Bartenstein P, Lieb K, Schreckenberger M. SPM-based count normalization provides excellent discrimination of mild Alzheimer's disease and amnestic mild cognitive impairment from healthy aging. NeuroImage. 2009; 44:43–50. [PubMed: 18691659]

Yezzi AJ Jr, Prince JL. An Eulerian PDE approach for computing tissue thickness. Med Imaging, IEEE Transact. 2003; 22:1332–1339.

Appendix A. Supplementary data

Supplementary data associated with this article can be found, in the online version, at doi: 10.1016/j.neuroimage.2010.04.033.

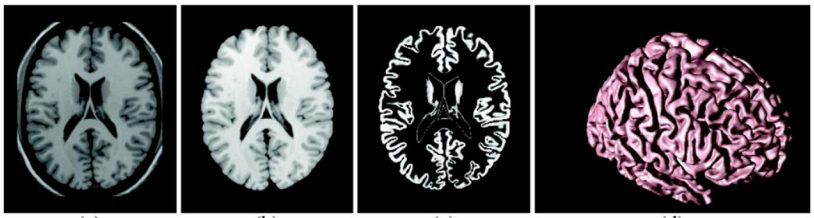

Fig. 1.

Geometric modeling of cerebral cortex: axial cross-section of (a) T1w MR image, (b) resulting cerebral volume, (c) resulting gray matter tissue segmentation, and (d) central cortical surface representation.

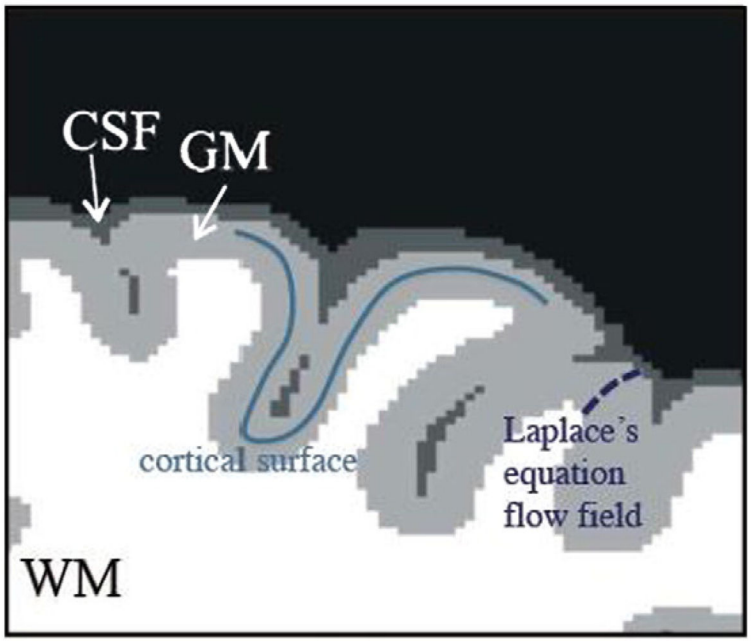

Fig. 2.

Schematic illustration of cortical thickness and rCBF computation. The Laplace's equation was solved in the GM mantle to estimate the flow field lines, uniquely connecting GM/WM and GM/CSF tissue boundaries. Local cortical thickness was estimated as the length of the Laplace's equation flow field lines and rCBF was integrated over the flow field lines to estimate rCBF.

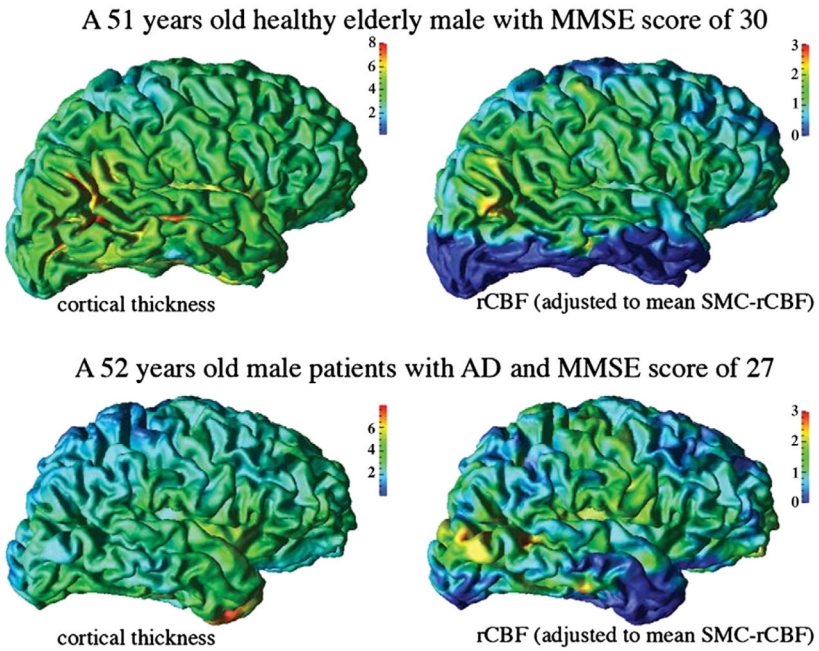

Fig. 3.

Representative cortical thickness and rCBF maps of a 51 year old healthy elderly male with a MMSE score of 30 (top row) and a 52 year old male AD patient with a MMSE score of 27 (bottom row). rCBF is corrected for tissue partial volume effects and also adjusted to mean rCBF of the sensory and motor cortex (SMC) to account for global variations in cerebral blood flow. Note further, the most inferior temporal lobe was not covered with arterial spin labeling MRI, because of technical limitations. Therefore, rCBF values in this region are set to zero.

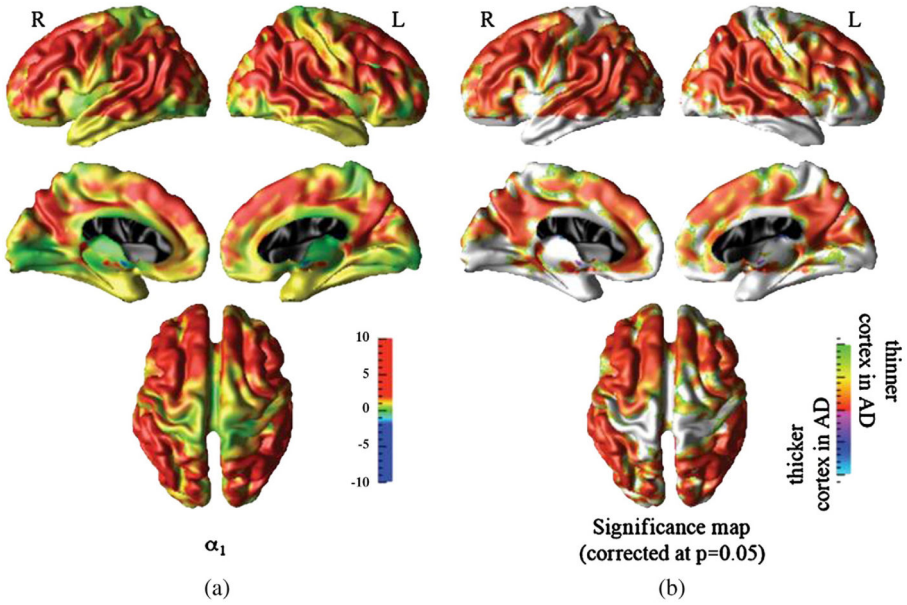

Fig. 4.

Classification power of cortical thinning for the binomial classification of CN and AD patients; (a) logistic regression coefficients and (b) significance map corrected at p=0.05.

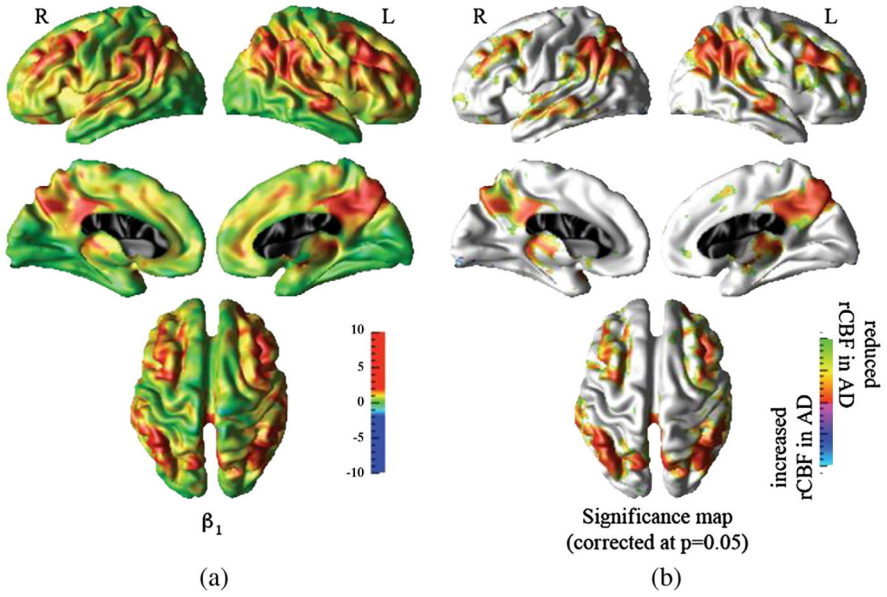

Fig. 5.

Classification power of reduced $rCBF_{PVE}$ for the classification of CN subjects and AD patients; (a) logistic regression coefficients and (b) significance map corrected at p=0.05.

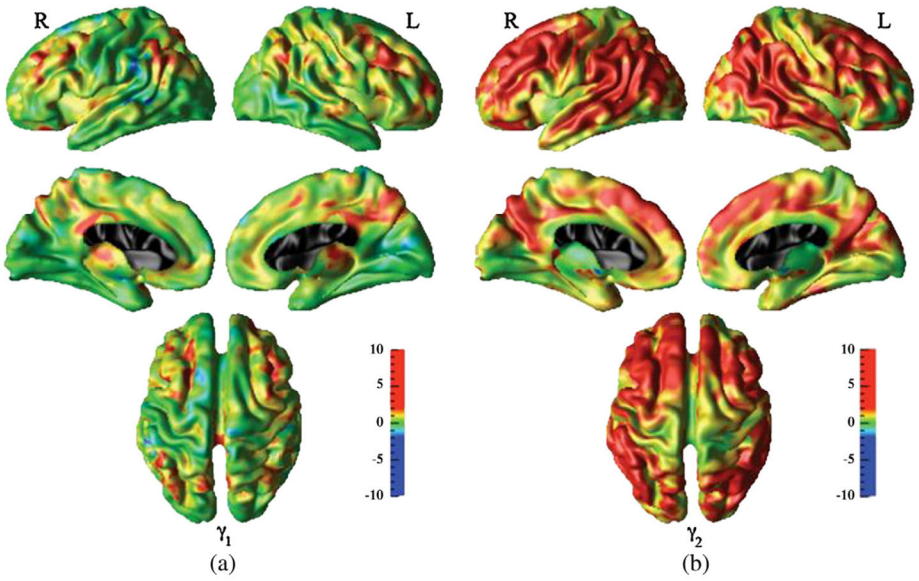

Fig. 6.

(a) $rCBF_{PVE}$ and (b) cortical thickness coefficients from a logistic regression analysis using $rCBF_{PVE}$, cortical thickness, and their interaction together for a correct classification of AD and control subjects.

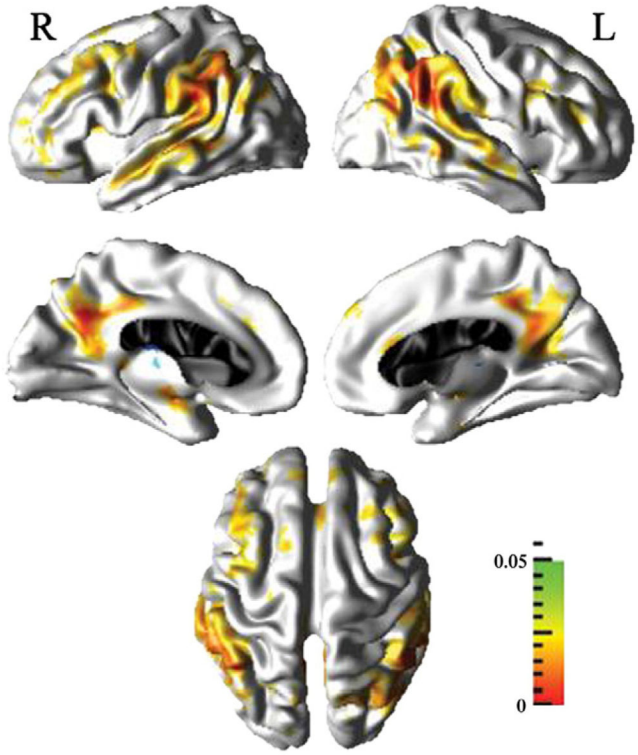

Fig. 7.

Cortical regions where cortical thinning significantly dominated rCBF in power for a correct classification of AD and CN.

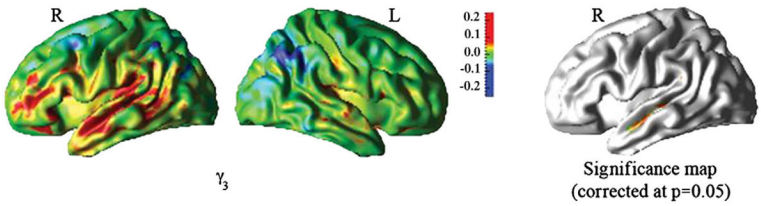

Fig. 8.

Maps of logistic regression coefficients (γ_3) using the interaction between reduced rCBF and cortical thinning for a correct classification between AD and CN and the corresponding significance map.

Table 1

Demographic features of study groups.

	Healthy elderly controls	Alzheimer's disease patients
Age (mean±std years)	65.70±8.25	66.29±9.99
Sex (F/M)	21/17	9/15
MMSE[a] (mean±std)	29.44±0.86	21.76±5.80

[a]Average MMSE of AD patients was significantly smaller than average MMSE of healthy elderly controls (Student's *t*-test, $p<10^{-9}$). There was no significant group difference in distribution of age (Student's *t*-test, $p=0.8$) or gender (Fisher's exact test, $p=0.2$).

Table 2

Explanatory power of regional cortical thinning or $rCBF_{PVE}$ for variability in MMSE in AD. Only regions of interest (sROI) with significant contributions are listed.

	R^2	β	Std error	*p*-value
Structural sROI				
Left temporal	0.542	1.793	0.24	$<10^{-6}$
Left parietal	0.481	1.627	0.25	$<10^{-6}$
Left cingulate	0.467	1.982	0.31	$<10^{-6}$
Right parietal	0.453	1.472	0.23	$<10^{-6}$
Right temporal	0.452	1.361	0.22	$<10^{-6}$
Left precuneus	0.449	1.413	0.23	$<10^{-6}$
Right precuneus	0.442	1.290	0.22	$<10^{-6}$
Right cingulate	0.395	1.782	0.32	$<10^{-5}$
Right frontal	0.372	2.390	0.46	$<10^{-4}$
Left frontal	0.365	2.847	0.55	$<10^{-4}$
Left entorhinal	0.296	0.643	0.15	$<10^{-4}$
Right entorhinal	0.286	0.959	0.23	$<10^{-4}$
Left cuneus	0.260	1.097	0.28	$<10^{-3}$
Right cuneus	0.174	0.771	0.26	0.005
All structural sROIs	*0.718*			$<10^{-5}$
Perfusion sROI				
Left precuneus	0.259	3.415	0.87	$<10^{-3}$
Right precuneus	0.234	3.162	0.87	$<10^{-3}$
Right parietal	0.196	2.411	0.75	0.002
Right temporal	0.185	3.812	1.24	0.003
Left parietal	0.176	1.902	0.64	0.005
Left temporal	0.170	3.318	1.15	0.006
Left posterior cingulate	0.096	1.683	0.91	0.068
Right posterior cingulate	0.071	1.222	0.86	0.162
Left parahippocampal gyrus	0.062	0.733	0.60	0.225
Right frontal	0.045	0.368	0.50	0.463
Right parahippocampal gyrus	0.042	0.331	0.53	0.535
Left frontal	0.040	0.237	0.43	0.580
All perfusion sROIs	*0.468*			*0.011*
Cumulative	*0.752*			$<10^{-4}$